Structural Flexibility of Non-Nucleoside HIV-1 Reverse Transcriptase Inhibitor: 9-Cl *TIBO* as Explained by Potential Energy Surface and ^{13}C and ^{1}H NMR Calculations, Based on *ab initio* and Density Functional Study

Suwipa Saen-oon,[†] Supa Hannongbua,*[,†] and Peter Wolschann[‡]

Laboratory for Computational & Applied Chemistry, Physical Chemistry Division, Chemistry Department, Faculty of Science, Kasetsart University, Bangkok 10900, Thailand, and Institute of Theoretical Chemistry and Structural Biology, University of Vienna, A-1090 Vienna, Austria

Received February 13, 2003

The conformational analysis of the HIV-1 reverse transcriptase inhibitor, (+)-(s)-4,5,6,7-tetrahydro-9-chloro-5-methyl-6-(3-methyl-2-butenyl)imidazol[4,5,1-*jk*][1,4]benzodiazepin-2(1*H*)-thione or 9-Cl *TIBO*, has been investigated using high level of calculations, *ab initio*, and DFT theory. The potential energy surface as the function of two important rotatable dihedral angles of the 9-Cl *TIBO* side chain was generated by the Hartree−Fock method at the 3-21G basis set. Eight pronounced local minima were found to exist within an energy difference of less than 10 kJ/mol. The energy barriers between the different local minima are lower than 15 kJ/mol. A second derivative (frequency) analysis showed that all conformers are stable at this level of theory. These structures were used as starting points for full geometry optimizations at the HF/6-31G** and B3LYP/6-31G** levels of theory to obtain the absolute geometries and structural information. The comparisons of calculated conformers with the bound conformer in the X-ray structure were sequentially considered. Additionally, to obtain some structural information and to correlate between calculated structures and the structure in solution, NMR chemical shift calculations were also performed on all eight local minimum structures at B3LYP/6-311++G** level, using the GIAO approach. The calculated ^{1}H NMR and ^{13}C NMR chemical shifts for the lowest energetic conformer give the greatest correspondence with the experimental results.

INTRODUCTION

Since the Human Immunodeficiency Virus Type 1 (HIV-1) was identified as the etiologic agent of the Acquired Immune Deficiency Syndrome (AIDS), the HIV-1 Reverse Transcriptase (RT) has become an attractive active target for several antiviral therapeutic agents used in the treatment of AIDS. The main biological function of HIV-1 RT is an essential enzyme involved in the life cycle of the HIV responsible for virus replication from single-stranded RNA viral genome into a double-stranded proviral DNA, which is then integrated into the host chromosome. During the past decade, several compounds with a wide variety of structures have been identified to counteract the activity of HIV-1 RT.[1−3] Non-nucleoside reverse transcriptase inhibitors (NNRTIs, such as nevirapine, delavirdine, tivirapine, and efavirenz) have, in addition to the nucleoside reverse transcriptase inhibitors (NRTIs) and protease inhibitors (PIs), been approved by the FDA to gain a definitive place in the treatment of HIV-1 infection.[4−8]

Evidently, numerous crystal structures of HIV-1 RT and complex with NNRTIs have indicated that the NNRTIs bind in the allosteric binding site which is located in the p66 palm subdomain of RT and is constituted mainly of hydrophobic residues.[9] The study of complex structures of HIV-1 RT with different NNRTIs makes it clear that although the NNRTIs are chemically diverse, they all bind at a common site in HIV-1 RT, and it reveals that there is a significant rearrangement of a three-stranded β-sheet in the p66 subunit with respect to the rest of the polymerase.[10,11] NNRTIs inhibit HIV-1 RT by inducing a conformational change of the enzyme to lock the polymerase active site (located in p66 palm subdomain and around 10−15 Å from the allosteric binding site around) into an inactive conformation. Furthermore, the shape of NNRTIs show a surprising similarity, sharing a common butterfly-like shape consisting of two (or more) wings, more specifically π-electron containing moieties, that do not share a common plane.[12] In general, the common structures of these π-systems for NNRTI analogues are aromatic rings as shown in Figure 1. However, it has been found that the derivatives of *TIBOs* cannot be fitted into the "two-hinged-ring" model in which one wing is simply a dimethylallyl moiety. 8-Cl *TIBO* (R86183) and 9-Cl *TIBO* (R82913) are considered as two of the most potent and selective inhibitors with high activity against HIV-1 RT. The 8-Cl *TIBO* or tivirapine is a derivative of tetrahydroimidazo[4,5,1-*jk*][1,4]benzodiazepinone which has been tested clinically and was discovered by Pauwels and co-workers in 1990.[13−15] Additionally, the high flexibility in the structure of the *TIBO* analogue plays an important role in the conformational changes for fitting into the binding pocket of HIV-1 RT to inhibit the enzyme process.

It is very important to understand the role of molecular structures of NNRTIs on HIV-1 RT inhibition; conformational analyses of potent NNRTIs such as HEPT, nevirapine, and derivatives of *TIBO* have been previously studied.[16−21]

* Corresponding author phone: +66-(2)-9428900; fax: +66-(2)-5793955; e-mail: fscisph@ku.ac.th.

[†] Kasetsart University.

[‡] Institute of Theoretical Chemistry and Structural Biology, University of Vienna.

10.1021/ci0340299 CCC: $25.00
Published on Web 08/08/2003

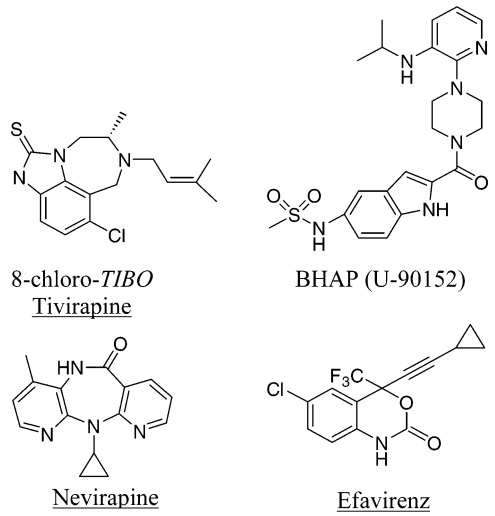

Figure 1. The structures of non-nucleoside reverse transcriptase inhibitors.

Therefore, an attempt has been made to investigate the conformational behavior of the 9-Cl *TIBO* in an extension of our studies as we have recently reported the conformational analysis of the 8-Cl *TIBO* compound using *ab initio* and DFT calculations.[22] The obtained results indicated the potential energy surface (PES) as the function of the two rotatable bonds of the dimethylallyl side chain using the HF/3-21G level. It was found that the geometry of the compound is mainly determined by the relative rigid aromatic ring system and the position of the side chain. We have determined two pronounced energetic local minimum regions of 8-Cl *TIBO* with a not very high energy barrier between both, estimated to be less than 20 kJ/mol, which allows an easy conformational change from one local minimum to the other. Moreover, it has been shown that the nitrogen inversion has some influences in the conformational change of 8-Cl *TIBO*. In *TIBO*s analogues, the biological activity against HIV-1 RT is decreased by changing the position of the Cl atom substituted on the aromatic ring at carbon 8 to be carbon 9 (8-Cl *TIBO*, 9-Cl *TIBO*) with the IC_{50} of 4.6 nM and 33 nM, respectively.[23] Therefore, to obtain some more structural information for the understanding of these effects, the energetic preferable conformations, and the conformational behavior of the inhibitor in the *TIBO* analogues, it is important to investigate the conformational analysis of the 9-Cl *TIBO* compound.

In this present study, the conformational analysis of 9-Cl *TIBO* was performed. This analysis was based on quantum chemical calculations with both *ab initio* and density functional theory (DFT) methods to explore the potential energy surface of the compound. The structure of 8-Cl *TIBO* as well as 9-Cl *TIBO* is mainly composed of three important parts, the benzoimidazole ring, the (S)-5-methyl substituent group, and the N6-dimethylallyl (DMA) side chain. Considering the DMA side chain as the most flexible moiety for the determination of the energetically possible conformations, the rotatable ability of this part must be calculated by an *ab initio* method, taking also into account conformational changes of the ring system. Exploring the PES of 9-Cl *TIBO* as the function of the two important rotatable bonds (N6−C15 and C15−C16) of the dimethylallyl side chain enables determination of the conformational space of 9-Cl *TIBO*. The chemical structure of 9-Cl *TIBO* together with the atomic numbering used in this investigation is given in Chart 1. Moreover, the DFT at B3LYP/6-311++G** level was used for calculation of the proton (^{1}H)-NMR and carbon (^{13}C)-NMR chemical shifts of 9-Cl *TIBO* in order to conceptualize the structure of the molecule in solution and compare it to the experimental data.[24]

Chart 1. (a) Chemical Structure of 9-Cl *TIBO* and Atomic Numbering and (b) The Three-Dimensional Structure of the Butterfly-like Shape of 9-Cl *TIBO*

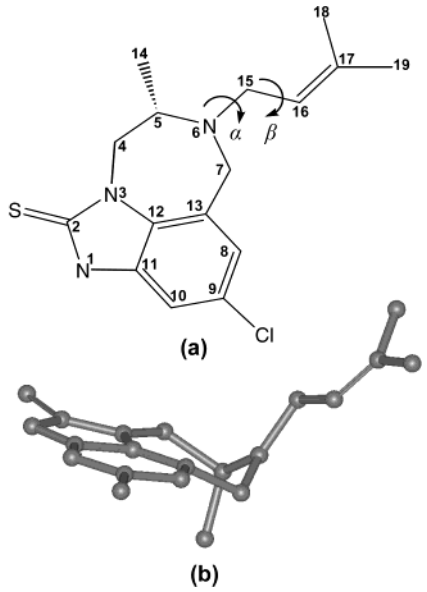

METHODS OF CALCULATION

The conformational analysis of 9-Cl *TIBO* compound was investigated based on quantum chemical calculations with *ab initio* as well as density functional theory (DFT) methods. The starting geometry of the 9-Cl *TIBO* structure was taken from the complex crystal structure of the enzyme HIV-1 RT and the 9-Cl *TIBO* inhibitor which is available in the Brookhaven Protein Data Bank with PDB entry code **1REV**.[25,26] Initially, the hydrogen atoms needed to be added to the extracted 9-Cl *TIBO* structure of the bound complex with HIV-1RT. Then, full geometrical optimization at the HF/3-21G level was carried out. All these calculations were done by GAUSSIAN98 program package[27] on a Cluster of Digital Alpha Servers (2100 4/275) of the University of Vienna. The obtained fully optimized structure was sequentially used as the starting geometry to produce the potential energy surface (PES) of 9-Cl *TIBO* at HF/3-21G level. The potential energy surface was mainly determined as the function of two rotatable bonds of the dimethylallyl side chain: alpha (α: C5−N6−C15−C16) and beta (*β*: N6−C15−C16=C17) (notation see Chart 1). The calculations were carried out by optimization of the geometries at fixed dihedral angles α and *β* by using the HF/3-21G level of theory. The *β* dihedral was varied with a step size of 30 degrees from 0 to 360 degrees, keeping the α dihedral angle constant with 30 degrees step size. This was repeated for different α dihedral angles also from 0 to 360 degrees with 30 degrees. Consequently, the full PES of 9-Cl *TIBO* was extrapolated as the three-dimensional plot between the dihedral angles α and *β* with the relative energy (kJ/mol) referring to differences with respect to the absolute minimum

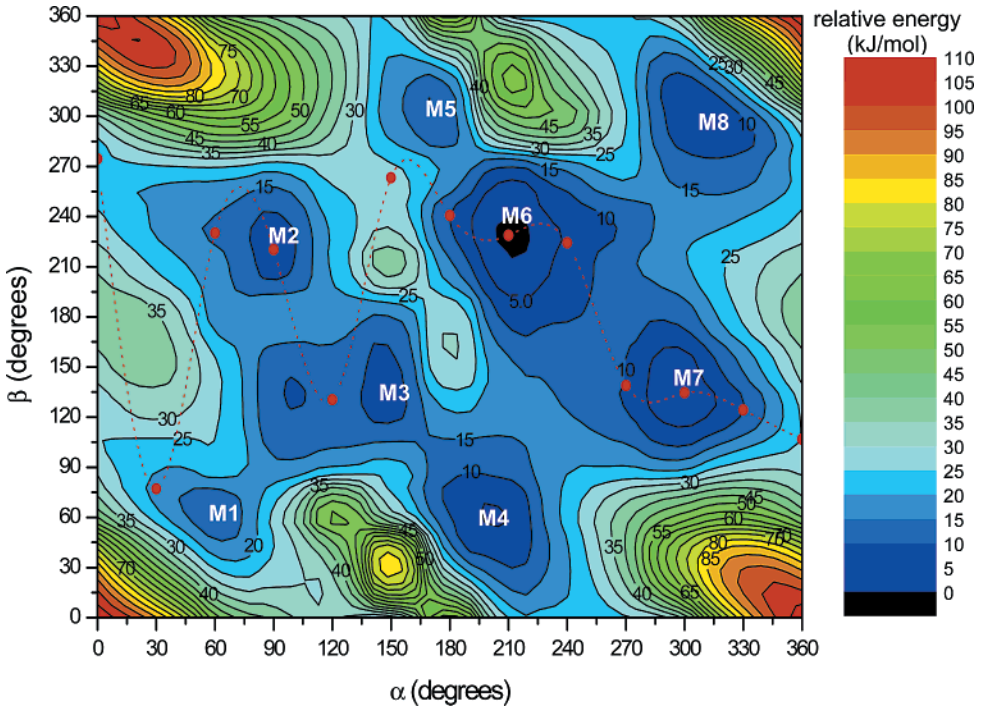

Figure 2. The potential energy surface (PES) of the 9-Cl *TIBO* calculated at the HF/3-21G level as a function of two variables: α and *β*, the C5−N6−C15−C16 and N6−C15−C16=C17 dihedral angles, respectively. Energy values (kJ/mol) refer to differences with respect to the absolute minimum. The projection of the rotational potential pathway at the HF/3-21G as the function of only dihedral angle α on the PES is represented by the red dash line with 30 degrees interval.

as shown in Figure 2. The interval of the relative energy level is 5 kJ/mol. The analysis of the PES was then performed to determine the energetically local minima and gain some significant conformational characteristics of the 9-Cl *TIBO* structure. The geometries of each local minimum existing on the PES were then fully optimized at the HF/3-21G, HF/6-31G**, and B3LYP/6-31G** levels of theory to obtain the absolute configuration of each local minimum structure. Furthermore, the harmonic frequency analyses were sequentially done on these fully optimized structures of all local minima for checking the characteristics of these minima. The frequency calculations were computed at the same level of calculations applied for the full optimizations, The zero point vibration energies (ZPVE) and relative free energies at 298 K and 1 atm were then obtained.

The ^{1}H NMR and ^{13}C NMR chemical shifts were calculated on the different conformational structures of 9-Cl *TIBO* belonging to each local minimum using the Gauge-Including Atomic Orbitals (GIAO) method implemented in the Gaussian98 program package.[28] The ^{1}H and ^{13}C chemical shielding constants of 9-Cl *TIBO*, $\sigma(^{1}H_i)$ and $\sigma(^{13}C_i)$, were computed at the B3LYP/6-311++G**//B3LYP/6-31G** level. The ^{1}H NMR and ^{13}C NMR chemical shifts, $\delta(^{1}H_i)$ and $\delta(^{13}C_i)$, are referred to a usual standard as TMS through the relation

$$\delta(^{1}H_i) = \sigma(^{1}H)_{TMS} - \sigma(^{1}H_i)_{TIBO} \quad (1)$$

$$\delta(^{13}C_i) = \sigma(^{13}C)_{TMS} - \sigma(^{13}C_i)_{TIBO} \quad (2)$$

where, to have accurate chemical shifts, the isotropic shielding constant of hydrogen and carbon atoms in TMS, $\sigma(^{1}H)_{TMS}$ and $\sigma(^{13}C)_{TMS}$, were calculated at the same computational level of the 9-Cl *TIBO* compound. Finally, the calculated ^{1}H NMR and ^{13}C NMR chemical shifts of all local minimum structures were compared to the experimental data.

In addition, solvation energies were calculated on the optimized geometries utilizing the self-consistent reaction field (SCRF)[29]method: integral equation formalism polarized continuum model (IEFPCM)[30] at the B3LYP/6-31G** level. In the model used, the solvent is assumed to be a continuous medium with a dielectric constant ϵ that surrounds a cavity, adjusted to fit the shape of the solute molecule to afford more accurate solvation energies. The dielectric constant for methanol ($\epsilon = 32.63$) was used as found in the experimental NMR chemical shifts investigation of the 9-Cl *TIBO* compound in perdeuterated methanol (CD_3OD) solution by Caldwell et al.[24] Therefore, in this study, the ^{13}C NMR chemical shifts calculations of the lowest energetic local minimum conformer included with the solvent effect were also performed using SCRF-IEFPCM solvation model.[31]

RESULTS AND DISCUSSION

The Potential Energy Surface. The conformational performance of the 9-Cl *TIBO* compound can be examined by the rotation and orientation in the space of the highly flexible DMA side chain. The potential energy surface or the hypersurface of the 9-Cl *TIBO* compound is shown in Figure 2 by varying two sensitive dihedral angles of the DMA side chain defined as alpha (α) and beta (*β*). The graphical presenting of the PES shows the high flexibility of the 9-Cl *TIBO* structure which is mainly due to the influence of the rotatable DMA side chain. The range of energetic fluctuation on the PES which is relative to the absolute energy is approximately 0−110 kJ/mol calculated at the HF/3-21G level. The large flat area for the energy less than 30 kJ/mol covers the range of α dihedral angle from 0 to 360 degrees and is approximately restricted

Table 1. Range of α and β Dihedral Angles, Lowest Energetic Grid of (α,β), and the Relative Energy (kJ/mol) of All Eight Local Minima from the PES

local minimum	range of dihedral angles[a] (degrees) α	β	lowest energetic grid[b] (degrees) (α,β)	relative energy[c] (kJ/mol)
M1	40−75	45−75	(60,60)	11.18
M2	80−105	200−240	(90,210)	8.33
M3	135−160	115−160	(150,120)	9.30
M4	175−220	30−90	(210,60)	5.33
M5	155−185	280−325	(180,300)	13.54
M6	180−265	170−270	(210,240)	0.00
M7	270−320	100−175	(300,150)	2.97
M8	290−340	275−325	(300,300)	6.17

[a] The estimated range of dihedral angle α and β determined graphically from the PES. [b] The lowest energetic grid (α,β) the increment of 30° of each local minima taken from the PES. [c] The relative energy of structure at the lowest energetic grids (α,β) with respect to the M6 and computed at HF/3-21G level.

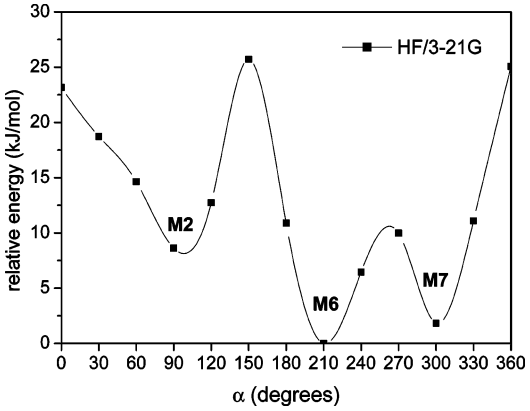

Figure 3. The rotational potential energy of α dihedral angle computed at the HF/3-21G level.

between 60 and 300 degrees for the β dihedral angle. Within this area, can be found eight pronounced local minima existing on the PES as depicted in Figure 2 and defined as M1, M2, M3, M4, M5, M6, M7, and M8. The range of α and β dihedral angles of all these eight local minima are determined graphically from the PES within the region of energy range 0−10 kJ/mol as shown in Table 1. From these eight local minima, the lowest energetic grids (α,β) at each local minimum are selected and give the relative energy with respect to the structural energy of local minimum M6.

The characteristics of all eight local minima have been checked by performing frequency calculations. The results show the characteristic performance of a local minimum, no imaginary frequency, for all eight local minima on the PES. Considering the relative energy, the M6 region can be defined as the lowest energetic local minimum which covers approximately 180−265 degrees for α and 170−270 degrees for β. The second local minimum is then identified in the M7 region with α at 270−320 degrees and β at 100−175 degrees with the higher energy of 3 kJ/mol. The energy barrier for conformational change between the lowest energetic minimum and the second minimum is lower than 15 kJ/mol which is clearly seen from the PES and the rotational potential in Figures 2 and 3, respectively.

Besides, the rotational potential of the 9-Cl *TIBO* compound as only the function of α dihedral angle was also calculated at the HF/3-21G level. The 9-Cl *TIBO* was partially optimized by keeping only the α dihedral angle constant while relaxing the rest of molecule. The α dihedral angle was varied from 0 to 360 degrees with the interval of 30°. In Figure 3, there are three pronounced local minima existing at dihedral angle α = 90, 210, and 300 degrees with the consistent dihedral angle β = 220, 228, and 134 degrees, respectively. The lowest energetic conformer is defined at dihedral angle α at 210 degrees (β = 228 degrees). All obtained three local minima are corresponding to the local minimum M2, M6, and M7 on the PES in Figure 2, but, eventually, these do not cover all other possible conformations. For example, at dihedral angle α 300°, there are two possible conformations existing on the PES with the dihedral angle β 150° and 300°, while the rotational potential (Figure 3) can be found with only one conformation. This rotational potential path of only varying dihedral angle α was also projected on the three-dimensional PES along the low energy regions as represented with the red dash line in Figure 2. It is obviously shown that the two-dimensional rotational potential of only varying the α dihedral angle is not sufficient to provide all possible local minimum structures in the case of a highly flexible molecule such as the *TIBO* structure compared to the three-dimensional PES. Therefore, the three-dimensional PES as the function of both α and β dihedral angles is more useful in obtaining better results of conformational behavior.

Table 2. Energies of the Eight Local Minimum Structures Calculated at B3LYP/6-31G** Level in kJ/mol[a]

structures	E^{rel}	E_0^{rel}	H_T^{rel}	G_T^{rel}	weight average[b]
M1	7.38	6.91	7.19	7.15	0.0559
M2	9.65	9.25	9.40	9.36	0.0229
M3	2.75	1.51	2.07	0.04	0.9832
M4	5.85	6.17	6.18	6.38	0.0762
M5	8.08	7.06	7.63	5.93	0.0912
M6	0.00	0.00	0.00	0.00	1.0000
M7	1.90	2.00	1.92	1.85	0.4742
M8	6.42	6.38	6.49	5.90	0.0925

[a] E^{rel} and E_0^{rel} are the internal energies without and with the zero point energy correction at 0 K; H_T^{rel} and G_T^{rel} are the enthalpies and Gibb free energies at T = 298 K and 1 atm. All relative energies (E^{rel}) are in kJ/mol. [b] Weight average (K) of Boltzmann distribution population: $N_{Mi}/N_{M6} = K = \exp[-\Delta G/RT] = \exp[-(G_{Mi}-G_{M6})/RT]$, where K is the ratio of mole fraction of the conformation M_i relative to M6, ΔG is their free energies difference, R = 8.314 J/mol·K, and T = 298 K (25 °C).

The absolute geometry of each individual local minimum was then performed by full optimization with higher level of calculations. The HF/6-31G** and B3LYP/6-31G** methods were applied for calculations of the accurate geometry at each local minimum. As shown in Table 2, the absolute conformation of M6 is the lowest energy conformer. We further investigated the zero-point vibrational energy (ZPVE) and thermal energy in the molecule, using the B3LYP/6-31G** calculations. The ZPVE corrections are within 1.30 kJ/mol (0.3 kcal/mol), as shown in Table 2. The results of some important dihedral angles and relative energies obtained from each method are presented in Table 3. Both HF and DFT methods at the 6-31G** basis set provide a high similarity for the geometries of all local minima and exactly the same energetic sequence of the minima in relation to relative energies as well. The absolute geometries of all eight local minima obtained by full optimization at the B3LYP/6-31G** level are illustrated in Figure 4.

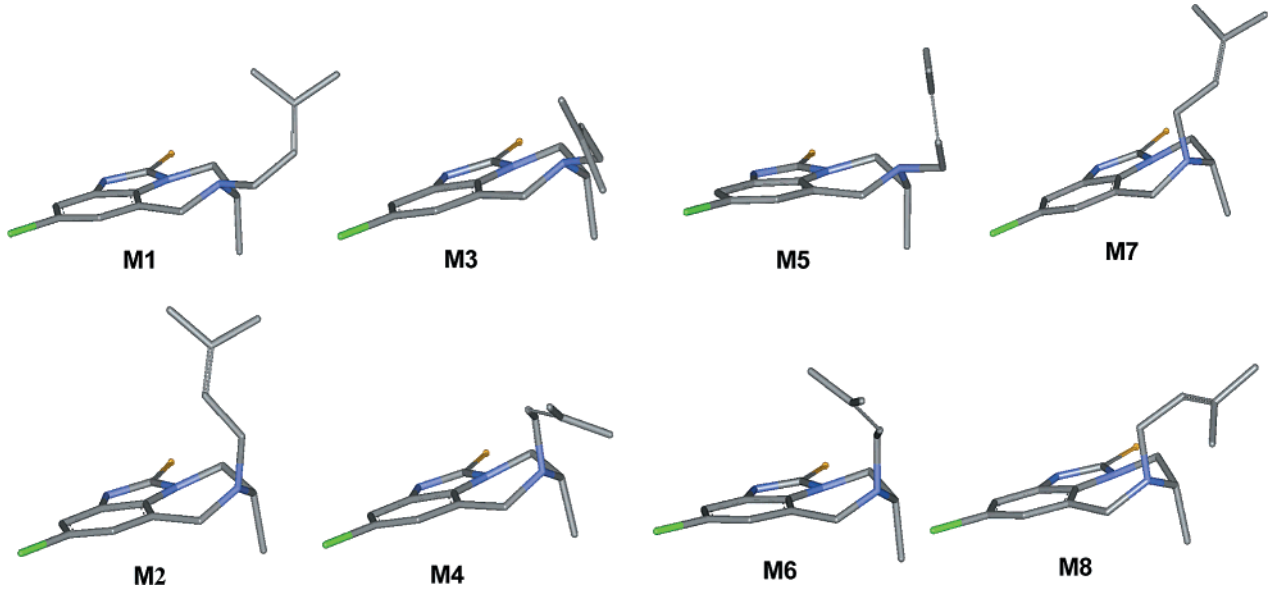

Figure 4. The conformation of eight local minimum structures obtained from the full optimization at the B3LYP/6-31G** level of theory.

Table 3. Comparison of the Selected Dihedral Angles of the Fully Optimized Geometries of All Eight Local Minima Obtained by HF and DFT Methods

local minimum	dihedral angles[a] (degrees)							
	α	β	N	A1	A2	A3	A4	A5
HF/6-31G**								
M1	59.3	71.0	131.1	219.3	88.6	166.7	61.1	37.0
M2	85.0	229.6	208.2	289.2	159.3	91.5	64.4	38.8
M3	156.8	132.5	131.8	219.2	88.5	165.1	61.0	39.2
M4	199.2	71.0	221.9	302.0	171.7	75.0	65.5	39.9
M5	168.0	287.4	130.2	218.6	87.8	167.6	60.8	38.6
M6	209.1	231.9	220.4	301.7	171.5	76.6	64.7	40.2
M7	300.2	135.7	220.0	302.1	171.8	75.5	66.1	38.5
M8	307.7	285.9	220.6	302.7	172.5	75.4	65.4	39.5
B3LYP/6-31G**								
M1	57.0	68.1	128.7	214.8	83.9	168.4	60.3	39.8
M2	79.2	227.8	211.4	290.0	160.2	87.4	63.6	42.4
M3	160.3	132.8	129.7	216.2	85.5	167.0	60.4	40.2
M4	195.6	68.3	223.0	302.5	172.2	73.3	64.6	41.6
M5	171.6	291.5	128.0	215.5	84.8	168.7	60.4	40.0
M6	206.3	231.8	222.1	302.2	172.0	74.8	64.0	41.6
M7	299.7	133.2	222.0	302.4	172.0	73.2	65.8	40.0
M8	307.5	289.3	223.0	303.2	172.8	72.5	64.8	42.1
X-ray Structure								
	185.5	171.1	193.0	286.2	161.5	81.6	68.2	21.7

[a] α: C5−N6−C15−C16; β: N6−C15−C16=C17; N: C5−N6−C7−C15; A1: C4−C5−N6−C15; A2: C14−C5−N6−C15; A3: C15−N6−C7−C13; A4: N3−C4−C5−C14; A5: C12−N3−C4−C5.

Considering the characteristic of the conformation of the lowest energy structure and of other local minimum ones, the relevant results on some important dihedral angles which represented the related positions of substituents, C5-Me and N6-DMA, to the seven-membered ring (diazepine ring) are depicted in Table 3. The dihedral angles A1 and A3 show the related position of the N6-DMA side chain to the diazepine ring, A2 and A4 indicate the related position of C5-Me to N6-DMA substituents and the diazepine ring, respectively, and N is a special notation for the nitrogen-inversion observation. Based on the geometrical similarity, all eight local minima can be classified into two groups, the first group containing the structures of M1, M3, and M5, and the second one containing the structures of M2, M4, M6, M7, and M8. Regarding the structural differences between the two groups by excluding the α and β dihedral angles, it reveals that two possibilities for the orientation of the DMA side chain connected to N6 exist as axial or equatorial. The position of C5-Me is kept as axial referring to the diazepine ring for both groups. The conformation of the diazepine ring is not changed from a twist-sofa conformer as observed with the A1 and A3 dihedral angles changes in Table 3 and in Figure 4. The superimposition of the selected representative conformers for the first and second group taken from the structure of M1 and M6, respectively, is shown in Figure 5. Nitrogen inversion at N6 can be observed between the structures of the two groups, and obviously it can be seen that the position of the lone-pair electron orbital of N6 points out to the opposite direction and, consequently, leads to the different stereochemistry of a chiral center N6. Therefore, the stereochemistry of N6 can be defined as R- and S-configuration for structures of the first and second group, respectively. It has been found that the X-ray structure in the bound complex with HIV-1 RT gives also that conformer of N6 which is similar to the calculated structures of the second group.[25] Regarding the energetic comparison between these two groups, it is shown that structures of the first group are less stable than some representative conformers of the second group such as M6, M7, M4, and M8 as indicated by the relative energies in Table 2. However, it is also observed that the highest energetic conformer is M2 of the second group which has an energy relative to the lower one of 11.75 kJ/mol, calculated at B3LYP/6-31G** level.

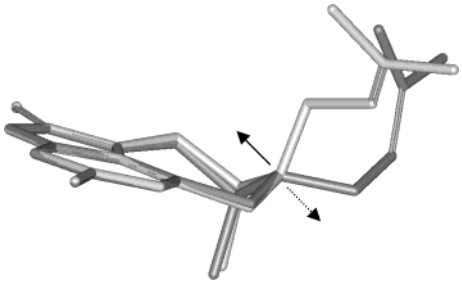

Figure 5. The superimposition of the representative structures of the first and second group as shown in light and dark gray, respectively. Arrows illustrate the conformational difference at N6 between the two groups.

Table 4. Energies for 9-Cl *TIBO* Local Minimum Structures Computed at the B3LYP/6-31G** Level in the Gas Phase and Solution Phase[a]

local minimum	$E^{\text{gas phase}}$	E^{iefpcm}	ΔG_{elec}	ΔG_{cav}	ΔG_{vdw}	ΔG_{sol} [b]
M1	−1644.42378	−1644.44696	−15.33	28.42	−27.64	−14.55
M2	−1644.42291	−1644.44468	−15.38	28.50	−26.77	−13.66
M3	−1644.42554	−1644.45002	−15.65	28.50	−28.21	−15.36
M4	−1644.42436	−1644.44689	−14.95	28.46	−27.64	−14.14
M5	−1644.42351	−1644.44595	−14.93	28.44	−27.59	−14.08
M6	−1644.42659	−1644.45033	−15.95	28.51	−27.46	−14.89
M7	−1644.42586	−1644.44877	−15.20	28.53	−27.70	−14.37
M8	−1644.42415	−1644.44776	−15.50	28.43	−27.75	−14.82

[a] The energies in solution phase are calculated utilizing the SCRF approach with IEFPCM solvation model. The dielectric constant of methanol solvent ($\epsilon = 32.63$). Energies (E) are in hartrees; all free energies changes (ΔG) are in kcal/mol. [b] $\Delta G_{\text{sol}} = \Delta G_{\text{elec}} + \Delta G_{\text{cav}} + \Delta G_{\text{vdw}}$.

The less stability of the structure of M2 might be due to the intramolecular steric interaction of the DMA side chain with the plane of the benzoimidazole ring and the strain in the alignment of its DMA side chain.

The obtained results of the free energy change of solvations for all eight local minimum conformers are given in Table 4. The solvation free energy (ΔG_{sol}) is defined as the free energy change to transfer a molecule from vacuum to solvent. The ΔG_{sol} can be considered to have three components, ΔG_{elec}, ΔG_{vdw}, and ΔG_{cav},where ΔG_{elec} stands for the electrostatic component, ΔG_{vdw} is the van der Waals interaction between the solute and the solvent, and ΔG_{cav} represents the free energy required to form the solute cavity within the solvent. The solvation free energies of all eight local minimum conformers are in the range of −13.66 to −15.36 kcal/mol and slightly different within 7.11 kJ/mol or 1.7 kcal/mol.

Comparison of the X-ray and Optimized Structures of Local Minima. To compare the calculated results with the experimental data, the structural parameters such as bond length, bond angle, and dihedral angle were compared for the X-ray and the calculated structures of eight local minima as shown in Table 5. Due to the minute variation between bond lengths and bond angles of eight local minimum structures compared to the X-ray structure, the standard deviation (SD) is presented (Table 5). The bond lengths between the structures of all eight local minima are not significantly different, and the deviations are less than 0.15 Å. The same results can be obtained for the bond angles within the maximum deviation of 8 degrees. The dramatic changes of the dihedral angles between all eight local minimum structures were found as shown in this table. For all eight local minimum structures, the benzoimidazole ring keeps planar, while the diazepine rings are adapted approximately 20 degrees above the plane of the benzoimidazole ring compared to the X-ray structure. These adaptable dihedral angles are shown in Table 5 with the bold numbers and are also illustrated with the superimposition in Figure 6(a). It sequentially makes the C5-Me substituent still conserve the axial position related to the diazepine ring. Therefore, the following can be observed: the similarity of the conformation of the core part, benzoimidazole ring, diazepine ring, and C5-Me, for all eight local minimum structures. However, we can discriminate the structures of the first and second groups from the orientation of the DMA side chain. It can be clearly seen as listed in Table 5 that the examined dihedral angles (C4−C5−N6−C15 and C13−C7−N6−C15) of the relative position of DMA side chain to the diazepine ring are different by about 70−80 degrees between the two groups and the second group is more structurally similar to the X-ray structure.

Figure 6(a) shows the superimposition of the X-ray structure and the lowest energetic local structure of M6. It is obviously illustrated that the orientation in space of the

Table 5. Comparison of the Structural Parameters of the X-ray and All Eight Local Minimum Structures of 9-Cl *TIBO* Taken from Full Optimization at the B3LYP/6-31G** Level

		the first group			the second group				
structural parameters	X-ray	M1	M3	M5	M2	M4	M6	M7	M8
bond lengths (Å)									
SD[a]		0.138	0.138	0.138	0.139	0.139	0.138	0.139	0.139
bond angles (degrees)									
SD		7.8	7.5	7.4	7.6	7.6	7.1	7.2	7.1
dihedral angles (degrees)[b]									
				Benzoimidazole Ring					
N1−C2−N3−C12	359.6	359.1	359.1	359.1	359.1	359.0	359.0	359.0	359.0
N1−C11−C12−N3	0.0	0.1	0.0	0.0	0.5	0.8	0.4	0.4	0.5
C11−N1−C2−N3	0.4	0.9	0.9	1.0	1.2	1.3	1.3	1.3	1.4
				Diazepine Ring					
C13−C12−N3−C4	**3.1**	**347.2**	**346.9**	**346.8**	**342.3**	**341.8**	**342.2**	**342.7**	**341.2**
C7−C13−C12−N3	**338.0**	**355.4**	**355.2**	**355.4**	**352.5**	**353.0**	**353.0**	**358.2**	**352.8**
C12−N3−C4−C5	**21.7**	**39.8**	**40.2**	**40.0**	**42.4**	**41.6**	**41.6**	**40.0**	**42.1**
N3−C4−C5−N6	302.1	287.9	288.0	287.9	293.7	294.2	293.7	295.4	294.1
C4−C5−N6−C7	92.9	87.9	88.0	88.1	78.4	79.6	79.9	79.8	79.1
C5−N6−C7−C13	**274.6**	**297.1**	**296.7**	**296.7**	**298.7**	**296.4**	**296.9**	**295.3**	**295.5**
				N6-DMA					
C5−N6−C15−C16 (α)	185.5	57.0	160.3	171.6	79.2	195.6	206.3	299.7	307.5
N6−C15−C16=C17 (β)	171.1	68.1	132.8	291.5	227.8	68.3	231.8	133.2	289.3
C4−C5−N6−C15	**286.2**	**214.8**	**216.2**	**215.5**	**290.0**	**302.5**	**302.2**	**302.3**	**303.2**
C13−C7−N6−C15	**81.6**	**168.4**	**167.0**	**168.7**	**87.3**	**73.3**	**74.8**	**73.3**	**72.5**
				C5-Me					
N3−C4−C5−C14	68.2	60.3	60.4	60.4	63.6	64.6	64.0	65.8	64.8
C14−C5−N6−C15	**161.5**	**83.9**	**85.5**	**84.8**	**160.2**	**172.2**	**172.0**	**172.0**	**172.8**

[a] Standard deviation (SD) = $[\sum(x_{\text{calc}} - x_{\text{expt}})^2/n - 1]^{1/2}$. [b] Atomic numberings are labeled in Chart 1.

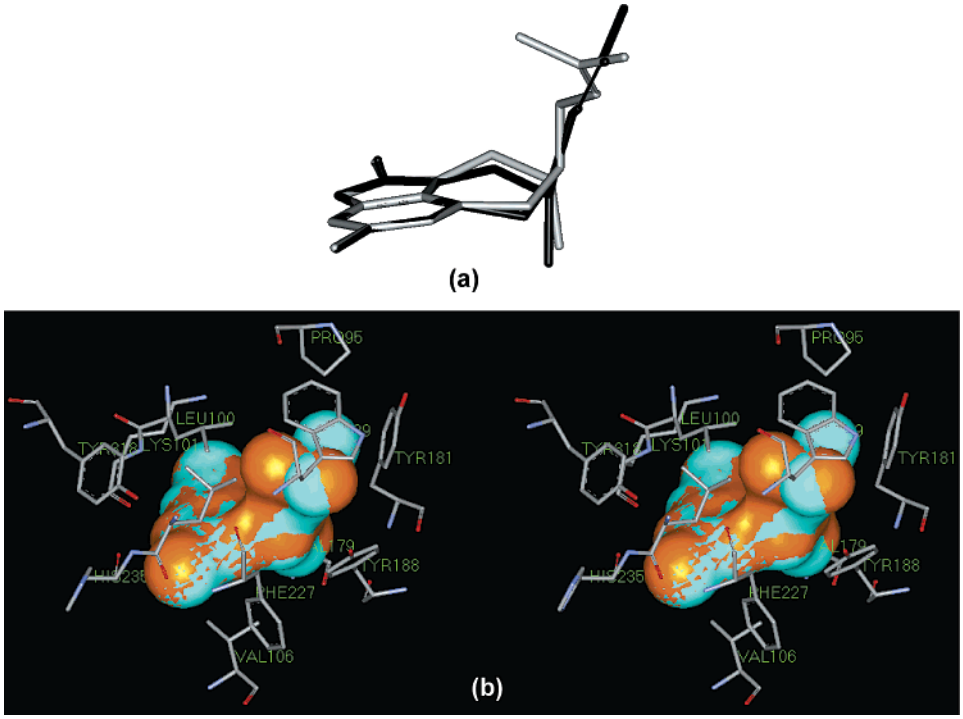

Figure 6. (a) The superimposition of the lowest energetic conformer and the X-ray structure as illustrated in light and dark gray, respectively. (b) The superimposition (stereoview) of the X-ray structure (blue) and the lowest energetic conformer (orange) into the NNIBP of HIV-1 RT as demonstrated with the solvent accessible surface of *TIBO*.

lowest energetic local structure corresponds to the structure of X-ray in the bound complex with HIV-1 RT. However, the differences of some dihedral angles of the diazepine ring and DMA side chain are also clearly demonstrated, especially for the adaptable stereochemistry of N6, which is enhanced sp^3 characteristic. This modification mainly causes the energy of the X-ray structure to be above the PES with an insignificant contribution from bond lengths and bond angles.

Additionally, it is also interesting to obtain some more information concerning the conformational characteristics of the calculated geometry compared to the X-ray structure which are bound into the binding pocket of HIV-1 RT, the so-called non-nucleoside inhibitor binding pocket (NNIBP). Therefore, the calculated structure of the lowest energetic conformer (M6) was then superimposed with the X-ray structure into the NNIBP, pdb entry code 1REV.[25] The picture of superimposition is given in Figure 6(b) to illustrate the similarity and diversity of the bound conformation to the NNIBP between calculated and X-ray structures. It shows the very good correspondence of calculated global structure to the X-ray structure.

Moreover, the interatomic distances between heavy atoms of both X-ray and calculated 9-Cl *TIBO* structures with the amino acid residues located in NNIBP which are closer than 4 Å were measured and demonstrated in Chart 2. The conformation of both X-ray and calculated structures are presented as the butterfly-liked shape combined with Wing I and Wing II. Although, the conformation of the calculated structure, obtained from M6, is adapted from the X-ray conformation, it still retains almost all of the interactions with amino acid residues in NNIBP. In particular, the interactions between some parts of the benzoimidazole ring (Wing I) and the close amino acid such as L100, K101, H235, and Y318 are still preserved which also include the H-bonding between N1−H of the imidazole ring of 9-Cl

Chart 2. Contact between Amino Acid Residues Surrounding the NNIBP and the 9-Cl *TIBO* Compound for Both the X-ray Conformation (in Bold) and the Lowest Energetic Conformation (M6, in Italics) within the Interatomic Distances ≤ 4 Å

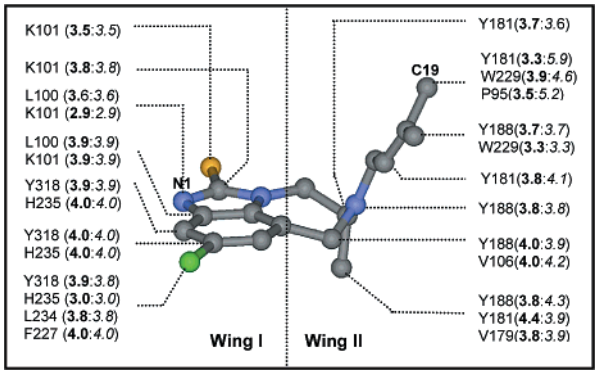

TIBO and C═O backbone of K101 with the distance of 2.9 Å. Besides, the interactions of Wing II with Y181, Y188, W229, V179, V106, and P95 are also conserved. Nevertheless, the different orientation of C19, which is a part of the DMA side chain, of the calculated structure induces the losing contact of some important van der Waal interactions to Y181, W229, and P95. It can be clearly seen from the superimposition in Figure 6(b) and the lengthened interatomic distances depicted in Chart 2.

^{13}C NMR and ^{1}H NMR Chemical Shifts Calculations of 9-Cl *TIBO*. Regarding the presentation of the potential energy surface of the 9-Cl *TIBO* compound obtained by the HF/3-21G method of calculation, it can be denoted that the high flexibility of this structure produces at least eight different conformers of eight local minima. To obtain the corresponding information of these various possible conformations to the conformational structure in solution, the NMR chemical shifts calculation was performed. In this study the ^{13}C NMR and ^{1}H NMR chemical shifts were calculated by

Table 6. Calculated ^{13}C NMR Chemical Shifts of Eight Local Minimum Structures Compared with Experimental Values

	chemical shifts (ppm)									
^{13}C NMR	M1	M2	M3	M4	M5	M6	M7	M8	$\bar{\delta}_{6,7}$ [b]	expt
C-2	181.45	182.86	180.56	182.12	181.33	181.96	182.57	182.66	182.62	168.80
C-4	59.91	58.06	60.08	53.13	59.57	53.68	52.16	52.49	52.33	52.39
C-5	55.10	61.93	64.62	60.48	62.39	61.26	54.27	53.38	53.83	55.82
C-7	59.52	55.34	54.30	51.39	54.29	51.18	58.10	57.87	57.99	53.43
C-8	124.58	124.52	127.46	126.26	127.80	125.60	126.14	125.29	125.72	122.09
C-9	143.71	144.33	142.83	145.01	144.90	144.70	144.57	144.75	144.66	129.00
C-10	109.52	109.95	108.98	109.80	108.83	110.06	110.04	110.09	110.07	108.21
C-11	137.53	137.15	137.55	137.16	137.35	137.49	137.45	137.52	137.49	131.26
C-12	137.06	137.99	137.35	138.68	137.02	137.81	137.71	137.52	137.62	130.75
C-13	132.42	139.02	131.99	132.47	130.68	133.50	134.30	134.58	134.44	125.66
C-14	5.48	18.51	8.55	18.74	6.81	19.14	19.24	17.77	18.51	17.60
C-15	56.28	60.74	60.51	50.83	57.88	52.65	53.27	51.31	52.29	46.58
C-16	125.78	134.33	132.70	126.78	127.26	130.93	131.25	126.54	128.90	121.27
C-17	155.96	142.27	146.82	154.66	155.20	146.82	147.20	154.83	151.02	136.06
C-18	27.72	27.73	27.81	27.47	27.61	27.71	28.05	27.40	27.73	25.86
C-19	20.23	17.58	19.00	19.59	20.25	18.45	19.34	19.45	19.40	17.86
SD [a]	***5.97***	***4.69***	***5.19***	***4.20***	***5.78***	***3.44***	***3.50***	***4.32***		

[a] Standard deviation (SD) = $[\sum(x_{calc} - x_{expt})^2/n-1\ ]^{1/2}$. [b] $\bar{\delta}_{6,7}$ chemical shifts correspond to Boltzmann weight average of M6 and M7 minimum structures.

Table 7. Calculated ^{1}H NMR Chemical Shifts of Eight Local Minimum Structures Compared with Experimental Values

	chemical shifts (ppm)								
^{1}H NMR	M1	M2	M3	M4	M5	M6	M7	M8	expt
H-4 (ax)[a]	3.39	4.14	3.68	3.97	3.76	3.92	3.64	3.78	4.18
H-4′(eq)	4.80	4.78	5.01	4.83	4.97	4.82	4.56	4.65	4.52
H-5[b]	3.41	3.36	3.06	3.30	2.98	3.29	3.45	3.60	3.55
H-7 (ax)	3.84	3.65	3.87	4.04	4.22	3.88	3.68	3.67	4.05
H-7′(eq)	4.21	4.81	3.54	4.21	3.51	4.25	4.66	4.59	4.25
H-8	6.82	6.75	6.88	6.86	6.98	6.36	6.92	6.91	6.88
H-10	6.75	6.83	6.71	6.74	6.63	6.64	6.79	6.73	7.07
H-14	0.91	1.36	1.08	1.42	1.07	1.42	1.36	1.25	1.31
H-15 (ax)	3.10	3.90	3.09	3.39	3.24	3.79	3.20	3.38	3.11
H-15′(eq)	3.29	3.73	3.59	3.17	2.99	2.96	3.93	3.53	3.21
H-16	5.54	5.57	5.61	5.68	5.58	5.51	5.57	5.65	5.20
H-18	1.88	1.52	1.82	1.84	1.84	1.80	1.87	1.82	1.74
H-19	1.88	1.66	1.76	1.83	1.98	1.52	1.68	1.85	1.46
SD	***0.37***	***0.36***	***0.32***	***0.26***	***0.38***	***0.32***	***0.29***	***0.31***	

[a] H (ax) is proton (H) at axial position and H (eq) is proton at equatorial position. [b] H-5 means proton connected to C-5.

the GIAO method at the B3LYP/6-311++G** level of theory on the optimized geometries of eight local minimum structures by B3LYP/6-31G** and compared with the experimental results. The corresponding calculated ^{13}C and ^{1}H NMR chemical shifts are summarized in Tables 6 and 7, respectively, together with the experimental data obtained in CD_3OD solution at room temperature by Caldwell et al.[24] For the consideration of the overall agreement between experimental and theoretical spectra, the correspondences between spectra patterns and trends as reflected by the standard deviation (SD) have been indicated to estimate the quality of the ^{13}C and ^{1}H NMR calculations as shown in Tables 6 and 7, respectively.

From the comparison of the calculated chemical shifts with the experimental values, the difference can be seen, as they are significantly smaller for the conformations of the second group (M2, M4, M6, M7, and M8) than the first group (M1, M3, and M5). Moreover, the correlations between the experimental and the calculated chemical shifts are better for the conformers in the second group than in the first group as indicated by the SD values. In particular, the SD values of ^{13}C NMR chemical shifts obviously show significant differences between these two groups and give the best correlation for the lowest energetic conformers, M6 and M7 as indicated by the SD values of 3.44 and 3.50, respectively. As reported by Caldwell et al.,[24] there are two possible conformational states due to during the NMR experiment the inhibitor can be changed to a different conformation. Therefore, in our study, the Boltzmann weight averages (Table 2) corresponding to the lowest energy minima are considered for both M6 and M7 conformers. The average chemical shifts of M6 and M7 ($\bar{\delta}_{6,7}$) were calculated and are reported in Table 6, indicating the most reliable conformers of M6 and M7.

It can be observed from the ^{13}C NMR chemical shifts that the significant different values are distributed by the C2, C4, C9, C14, C16, and C17 approximately in the range of 10−20 ppm. These carbon atoms are bonded to the S, N, Cl, and the double bond which affect the large different electronic environment for the calculated structures in the gas phase, compared to the experimental structure in solution. However, the other connected C−C atoms give small differences less than 3 ppm, and it shows the very high correlation between calculated and experimental values as given in Table 6. Therefore, the solvent effects are taken into account to calculate the ^{13}C NMR chemical shifts of the lowest energetic conformer (M6) using the SCRF-IEFPCM solvation model with the dielectric constant for methanol ($\epsilon = 32.63$). This NMR chemical shifts calculation was carried out on the same optimized geometry of M6 used in the gas-phase calculation at the B3LYP/6-311++G** level. The results show the improvement of the ^{13}C NMR chemical shifts of some significantly sensitive carbons by including the solvent effect as listed in Table 8.

The poor correlation with the first group is influenced by the greater differences in values of both the^{13}C and ^{1}H NMR chemical shifts of C4 which are affected by the orientation in space of the lone-pair electronic orbital of N6 pointed into the diazepine ring system. Moreover, the inconsistent position of the C5-methyl substituent (C14) for the conformers in the first group compared to the X-ray structure also gives the larger different value of C14 chemical shifts (9−12 ppm) than the conformers in the second group (less than 2 ppm). The achieved ^{13}C NMR chemical shifts results beneficially support the agreement that the second group is the preferable conformation in solution. In particular, for the

Table 8. ^{13}C NMR Chemical Shifts of the Lowest Energetic Conformer (M6) in Gas Phase and Solution Phase

	gas phase		solution phase[a]		
carbon	calc	residual	calc	residual	expt
C-2	181.96	−13.16	170.83	−2.03	168.80
C-9	144.70	−15.70	147.62	−18.62	129.00
C-12	137.81	−7.06	134.55	−3.80	130.75
C-14	19.14	−1.54	18.59	−0.99	17.60
C-16	130.93	−9.66	122.91	−1.64	121.27
C-17	146.82	−10.76	139.61	−3.55	136.06

[a] Solution phase was performed in the SCRF-IEFPCM solvation model.

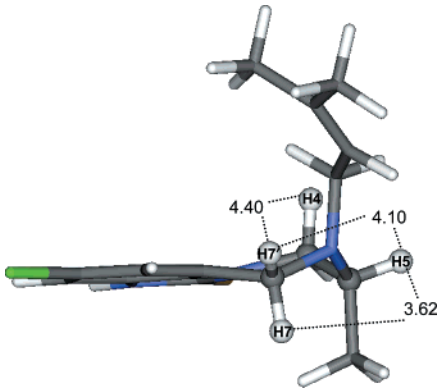

Figure 7. The approximate NOE observation on the conformation of M6 structure by measuring the distances between the two protons.

lowest energetic conformer (M6) yields, the ^{13}C NMR and ^{1}H NMR chemical shift values of the side chain shows the best correlation to the experimental values. According to the experimental NMR investigation from Caldwell et al., they observed an NOE between H-5 and H-7 protons; however, no NOE was observed between H-4 and H-7′ protons. As an NOE considered the proton−proton interaction through space within the distance of 4 Å, we attempted to approximately observe an NOE by measuring the distances. Thus, the distances of these concerned protons of the lowest energetic conformer (M6) were measured and presented in Figure 7. The distance between H-5 and H-7 protons is 3.62 Å that could be implied to observe an NOE between these two protons. The distance between H-4 and H-7′ protons is larger than 4 Å, thus, it can be assumed that no NOE might be observed. Therefore, the conformation of the lowest energetic conformer of M6 obtained from this study corresponds well to the conformation in solution of the experimental data.

The results of M1 and M6 were selected as the representative for the first and second groups, respectively, to show the correlation plot between the calculated and experimental ^{13}C and ^{1}H NMR chemical shifts as shown in Figure 8(a),-(b), respectively, together with the correlation coefficient (R^2). A more quantitative comparison between calculated and experimental chemical shifts can be performed by considering the agreement between spectra patterns and general trends. For the ^{13}C NMR and ^{1}H NMR prediction, it can be noted that the GIAO method can provide reasonable results which are rather corresponding to the experimental ones, as linear relations are shown in Figure 8. Additionally, the

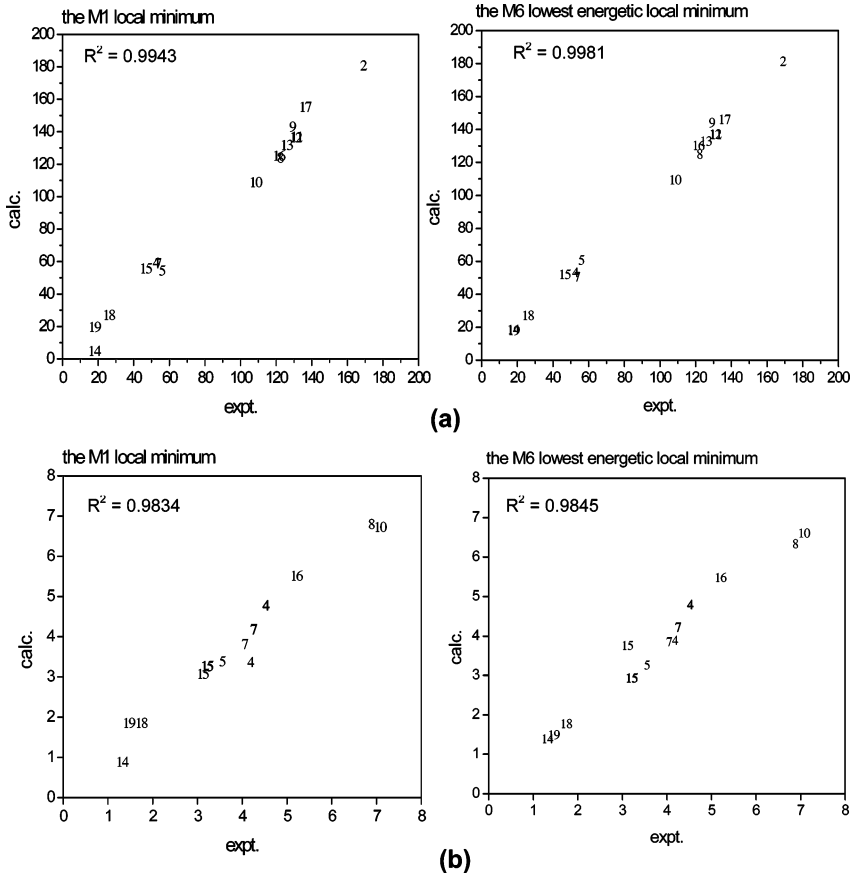

Figure 8. Correlation plot between calculated and experimental chemical shifts for the M1 and M6 representative conformers of the first and second groups, respectively. (a) ^{13}C NMR correlation and (b) ^{1}H NMR correlation; ^{1}H-equatorial positions are presented with the **bold** such as H-4′ and H-7′.

results from the ^{1}H NMR chemical shifts calculations are also taken into account as presented in Table 7 and Figure 8(b). It is observed that the standard deviation of ^{1}H NMR chemical shifts gives slightly inconsistent results of any conformers in the first and second group as found in the ^{13}C NMR prediction. This might be due to the high sensitivity of the ^{1}H NMR chemical shifts and mainly depends on the geometry together with the solvent effect comparison to the experiment.

CONCLUSIONS

The performance of conformational analysis on the 9-Cl *TIBO* inhibitor based on quantum chemical calculations gives eight pronounced low energetic conformational minima on the potential energy surface. The local minimum structures can be classified into two groups based on the orientation of side chain and the influence of the stereochemistry on N6. The representative conformations of the second group show more stable structures. It has been found that the lowest energetic conformer belongs to the second group and appears at dihedral angles of α and β equal to 206.28 and 231.78 degrees, respectively. It is found from our study that the two-dimensional rotational potential of only varying the α dihedral angle is not sufficient to provide all possible local minimum structures in the case of a highly flexible molecule such as the *TIBO* structure compared to the three-dimensional PES. The three-dimensional PES as the function of both α and β dihedral angles is useful in obtaining information on the conformational behavior of the molecules. Based on the 9-Cl *TIBO* structure which is mainly focused on the conformational space, the obtained results indicate that the lowest energetic conformation corresponds well to the geometry of the bound conformation in the complex structure with HIV-1 RT. Moreover, the ^{13}C and ^{1}H NMR chemical shift calculations also agree well with the conformation found in the solution. We obtained structural information of the HIV-1 RT in the class of *TIBO* derivatives that the inhibitor should contain the flexibility part in the molecule in order to easily allow the conformational change upon binding for fitting into the binding cavity. Based on the adapted conformer bound in the complex, the inhibitor should contain two π-electron moieties or wings, connected by the highly flexible part as easy to rotate or adapt its structure to show important interactions with amino acid residues in the binding pocket. The configuration of the N6 should be retained as the S-configuration to lead the orientation of the DMA side chain for preserving the van der Waal interaction with the binding pocket. The discrimination of different biological activity based on different conformations of 8-Cl and 9-Cl *TIBO* bound to the HIV-1 RT complexes is needed for the next investigation.

ACKNOWLEDGMENT

S. Hannongbua is grateful to the Thailand Research Fund and KURDI for a research fellowship (RSA4480001). S. Saen-oon is also grateful to the Royal Golden Jubilee Ph.D. Program (3.C.KU/42/B.1) and to the *development cooperation of the Republic of Austria* within the *Scholarship program* 894/00, *Nord-Süd-Dialog-Stipendienprogramm* 2000/01. The Postgraduate on Education and Research in Petroleum and Petrochemical Technology (ADB-MUA), the high performance computing centers of Kasetsart University, the National Electronics and Computer Technology (HPCC/NECTEC), and the computer center of the University of Vienna are also gratefully acknowledged for the generous allocation of computer resources. Anthony Reardon is also grateful for reading of the manuscript.

REFERENCES AND NOTES

(1) Arnold, E.; Das, K.; Yadav, P. N. S.; Hsiou, Y.; Boyer. P. L.; Hughes, S. H. Targeting HIV Reverse Transcriptase for Anti-AIDS Drug Design. *Drug. Des. Discov.* **1996**, *13*, 29−47.

(2) De Clercq, E. The Role of Nonnucleoside Reverse Transcriptase Inhibitors (NNRTIs) in the Therapy of HIV-1 Infection. *Antiviral Res.* **1998**, *38*, 153−179.

(3) Jonckheere, H.; Anne, J.; De Clercq, E. The HIV-1 Reverse Transcription (RT) Process as Target for RT Inhibitors. *Med. Res. Rev.* **2000,** *20*, 129−154.

(4) Merluzzi, V. J.; Hargrave, K. D.; Labadia, M.; Grozinger, K.; Skoog, M.; Wu, J. C.; Shih, C. K.; Eckner, K.; Hattox, S.; Adams, J.; Rosenthal, A. S.; Faanes, R.; Eckner, R. J.; Koup, R. A.; Sullivan, J. L. Inhibition of HIV-1 Replication by Nonnucleoside Reverse Transcriptase Inhibitor. *Science* **1990**, *250*, 1411−1413.

(5) Young, S. D. Nonnucleoside Inhibitors of HIV-1 Reverse Transcriptase. *Perspect. Drug Discov. Des*. **1993**, *47*, 155−169.

(6) De Clercq, E. Antiviral Therapy of Human Immunodeficiency Virus Reverse Infection. *Clin. Microbiol. Rev.* **1995**, *8*, 200−239.

(7) Patel, M.; Ko, S. S.; Mchugh, R. J., Jr.; Markwalder, J. A.; Srivastava, A. S.; Cordava, B. C.; Klabe, R. M.; Ericson-Viitanen, S.; Trainor, G. L.; Seitz, S. P. Synthesis and Evaluation of Analogues of Efavirenz (SUSTIVA) as HIV-1 Reverse Transcriptase Inhibitors. *Bioorg. Med. Chem. Lett*. **1999**, *9*, 2805−2810.

(8) Tachedjian, G.; Orlova, M.; Sarafianos, S. G.; Arnold, E.; Goff, S. P. Nonnucleoside Reverse Transcriptase Inhibitors are Chemical Enhancers of Dimerization of the HIV Type 1 Reverse Transcriptase. *Proc. Natl. Acad. Sci.* **2001**, *98*, 7188−7193.

(9) Tantillo, C.; Ding, J. P.; Jacobo Molina, A.; Nanni, R. G.; Boyer, P. L.; Hughes, S. H.; Pauwels, R.; Andries, K.; Janssen, P. A. J.; Arnold, E. Locations of Anti-AIDs Drug Binding Sites and Resistance Mutations in the 3-Dimensionals Structure of HIV-1 Reverse Transcriptase: Implication for Mechanisms of Drug inhibition and Resistance. *J. Mol. Biol*. **1994**, *243*, 369−387.

(10) Esnouf, R.; Ren, J.; Ros, C.; Jones, Y.; Stammers, D.; Stuart, D. Mechanism of inhibition of HIV-1 Reverse Transcriptase by Nonnucleoside Iinhibitors. *Struct. Biol*. **1995**, *2*, 303−308.

(11) Madrid, M.; Jacobo-Molina, A.; Ding, J.; Arnold, E. Major Subdomain Rearrangement in HIV-1 Reverse Transcriptase Simulated by Molecular Dynamics. *Protein-Struct. Funct. Genet*. **1999**, *35*, 332−337.

(12) Ding, J.; Das, K.; Moereels, H.; Koymans, L.; Andries, K.; Jannsen, P. A. J.; Hughes, S. H.; Arnold, E. Structure of HIV-1 RT/TIBO R86183 Complex Reveals Similarity in the Binding of Diverse Nonnucleoside Inhibitors. *Struct. Biol*. **1995**, *2*, 407−415.

(13) Pauwels, R., Andries, K.; Desmyter, J.; Schols, D.; Kukla, M. J.; Breslin, H. J.; Raeymaeckers, A.; Van Gelder, J.; Woestenborghs, R.; Heykants, J.; Schellekens, K.; Janssen, M. A. C.; De Clercq, E.; Janssen, P. A. J. Potent and Selective Inhibition of HIV-1 Replication in Vitro by a Novel Series of TIBO Derivatives. *Nature* **1990**, *343*, 470−474.

(14) Buckheit, R. W.; Germany-Decker, J.; Hollingshead, M. G.; Allen, L. B.; Shannon, W. M.; Janssen, P. A. J.; Chirigos, M. A. Differential Antiviral Activity of two TIBO derivatives Against the Human Immunodeficiency and Marine Leukemia Viruses Alone and in Combination with Other Anti-HIV Agents. *AIDS. Res. Hum. Retroviruses* **1993**, *9*, 1097−1106.

(15) Pauwels, R.; Andries, K.; Debyser, Z.; Kukla, M. J.; Schols, D.; Breslin, H. J.; Woestenborghs, R.; Desmyter, J.; Janssen, M. A. C.; De Clercq, E.; Janssen, P. A. J. New Ttetrahydroimidazo[4,5,1-*jk*]-benzodiazepin-2(1*H*)-one and -thione derivatives are Potent Inhibitors of Human Immunodeficiency Virus Type 1 Replication and are Synergistic with 2′,3′-dideoxynucleoside Analogs. *Antimicrob. Agents Chemother*. **1994**, *38*, 2863−270.

(16) Lawtrakul, L.; Hannongbua, S.; Beyer, A.; Wolschann, P. Conformational Study of the HIV-1 Reverse Transcriptase Inhibitor 1-[(2-Hydroxyethoxy)methyl]-6-(phenylthio)thymine (HEPT). *Biol. Chem*. **1999**, *380*, 265−267.

(17) Hannongbua, S.; Prasitthichokekul, S.; Pungpo, P. Conformational Analysis of Nevirapine, a Non-nucleoside HIV-1 Reverse Transcriptase

Inhibitor, Based on Quantum Mechanical Calculations. *Compt.-Aided Mol. Des*. **2001**, *15*, 997−1004.
(18) Mui, P. W.; Jacober, S. P.; Hargrave, K. D.; Adams, J. Crystal Structure of Nevirapine, a Nonnucleoside Inhibitor of HIV-1 Reverse Transcriptase, and Computational Alignment with a Structurally Diverse Inhibitor. *J. Med. Chem.* **1992**, *35*, 201−202.
(19) Schaefer, W.; Friebe, W. G.; Leineert, H.; Mertens, A.; Poll, T.; Von der Saal, W.; Silch, H.; Nuber, B.; Ziegler, M. L. Non-nucleoside Inhibitors of HIV-1 Reverse Transcriptase: Molecular Modeling and X-ray Structure Investigations. *J. Med. Chem*. **1993**, *36*, 726−732.
(20) Peeters, A.; Van Alsenoy, C.; Dillen, J.; Geise, H. J. Ab initio Study of Tetrahydro-imidazo[4,5,1-jk][1,4]-benzodiazepin-2(1H)-one and -thione (TIBO) Derivatives R79882 and R82913. *J. Mol. Struct. (THEOCHEM)* **1995**, *333*, 99−110.
(21) Parreira, R. L.; Abrahao, O., Jr.; Galembeck, S. E. Conformational Preferences of Non-nucleoside HIV-1 Reverse Transcriptase Inhibitors. *Tetrahedron*. **2001**, *57*, 3243−3253.
(22) Hannongbua, S.; Saen-oon, S.; Pungpo, P.; Wolschann, P. Molecular Calculations on the Conformation of the HIV-1 Reverse Transcriptase Inhibitor (+)−(s)-4,5,6,7-Tetrahydro-8-chloro-5-methyl-6-(3-methyl-2-butenyl)-imidazol[4,5,1-*jk*][1,4]benzodiazepin-2(1*H*)-thione (8-Chloro-*TIBO*), *Monatsh. Chem.* **2001**, *132*, 1157−1169.
(23) Das, K.; Ding, J.; Hsiou, Y.; Clark, A. D., Jr.; Moereels, H.; Koymans, L.; Andries, K.; Pauwels, R.; Janssen, P. A.; Boyer, P. L.; Clark, P.; Smith, R. H., Jr.; Kroeger Smith, M. B.; Michejda, C. J.; Hughes, S. H.; Arnold, E. Crystal Structures of 8-Cl and 9-Cl TIBO Complexed with Wild-Type HIV-1 RT and 8-Cl TIBO Complexed with the Tyr181Cys HIV-1 RT Drug-Resistant Mutant. *J. Mol. Biol*. **1996**, *264*, 1085−1100.
(24) Caldwell, G. W.; Guathier, A. D.; Leo, G. C.; Kukla, M. J. Conformational Analysis of the Reverse Transcriptase Inhibitor (+)−(S)-4,5,6,7-tetrahydroimidazo-9-chloro-5-methyl-6-(3-methyl-2-butenyl)imidazo[4,5,1-jk][1,4]-benzodiazepin-2-thione (TIBO; R82913). *Tetrahedron Lett*. **1993**, *34*, 2063−2066.
(25) Ren, J.; Esnouf, R.; Hopkims, A.; Ross, C.; Jone, Y.; Stammers, D.; Stuart, D. The Structure of HIV-1 Reverse Transcriptase Complexed with 9-chloro-TIBO: Lessons for Inhibitor Design. *Structure* **1995**, *3*, 915−926.
(26) Berman, H. M.; Westbrook, J.; Feng Z.; Gilliland, G.; Bhat, T. N.; Weissig, H.; Shindyalov, I. N.; Bourne, P. E. The Protein Data Bank. *Nucleic Acids Res*. **2000**, *28*, 235−242. (http://pdb.bnl.gov/).
(27) Frisch, M. J.; Trucks, G. W.; Schlegel, H. B.; Scuseria, G. E.; Robb, M. A.; Cheeseman, J. R.; Zakrzewski, V. G.; Montgomery, J. A.; Stratmann, R. E.; Burant, J. C.; Dapprich, S.; Millam, J. M.; Daniels, A. D.; Kudin, K. N.; Strain, M. C.; Farkas, O.; Tomasi, J.; Barone, V.; Cossi, M.; Cammi, R.; Mennucci, B.; Pomelli, C.; Adamo, C.; Clifford, S.; Ochterski, J.; Petersson, G. A.; Ayala, P. Y.; Cui, Q.; Morokuma, K.; Malick, D. K.; Rabuck, A. D.; Raghavachari, K.; Foresman, J. B.; Cioslowski, J.; Ortiz, J. V.; Fox, D. J.; Keith, T.; Al-Laham, M. A.; Peng, C. Y.; Nanayakkara, A.; Gonzalez, C.; Challacombe, M.; Gill, P. M. W.; Johnson, B. G.; Chen, W.; Wong, M. W.; Andres, J. L.; Head-Gordon, M.; Replogle, E. S.; Pople, J. A.; Gaussian 98 (Version A.1); Gaussian Inc.: Pittsburgh, PA, 1998.
(28) Wasikowski, K.; Hilton, J. F.; Pulay, P. Efficient Implementation of The Gauge Independent Atomic Orbital Method for NMR Chemical Shift Calculations. *J. Am. Chem. Soc*. **1990**, *112*, 8251−8262.
(29) Cramer, C. J.; Truhlar, D. G. Continuum Solvation Models: Classical and QuantumMechanical Implementations. *Reviews in Computational Chemistry*; Kipkowitz, K. B., Boyd D. B., Eds.; VCH: New York, 1995; Vol. 6, pp 1−72.
(30) Tomasi, J.; Mennucci, B.; Cances, E. The IEF version of the PCM solvation method: an overview of a new method addressed to study molecular solutes at the QM ab initio level. *J. Mol. Struct. (THEOCHEM)*. **1999**, *464*, 211−226.
(31) Helgaker, T.; Jaszunski, M.; Ruud, K. Ab initio Method for the Calculation of NMR Shielding and Indirect Spin−Spin Coupling Constants. *Chem. Rev.* **1999**, *99*, 293−352.

CI0340299